Polymer 51 (2010) 2191–2198

Contents lists available at ScienceDirect

Polymer

journal homepage: www.elsevier.com/locate/polymer

Morphology control of segmented polyurethanes by crystallization of hard and soft segments

Matthew A. Hood [a], Bingbing Wang [a], James M. Sands [b], John J. La Scala [b], Frederick L. Beyer [b], Christopher Y. Li [a,*]

[a] Department of Materials Science and Engineering, Drexel University, Philadelphia, PA 19104, United States
[b] Army Research Laboratory, Aberdeen Proving Ground, MD 21005, United States

ARTICLE INFO

Article history:
Received 1 February 2010
Received in revised form
11 March 2010
Accepted 13 March 2010
Available online 20 March 2010

Keywords:
Segmented polyurethane
Confined crystallization
Phase separation

ABSTRACT

Segmented polyurethanes (SPUs) have been designed with controlled hard to soft segment ratios. The confinement effect of the SPU blocks is induced by phase separation of the SPU segments and has been harnessed to selectively control crystallization. Hard segment (HS) concentrations greater than 50 wt.% allowed for the study of morphological changes and mechanical properties associated with confinement of the soft segment (SS). It was observed that crystallization temperature and normalized percent crystallinity were reduced with increasing HS content, creating a largely amorphous PEG SS at ambient temperature. High temperature annealing further confined the SS because the HS had more time to crystallize, which increased confinement. Considerable insight has been gained through the manipulation and characterization of the SS and HS, in an SPU, towards the design of impact absorbing and structural materials.

1. Introduction

Segmented polyurethanes (SPUs) are a versatile class of material possessing various controllable properties. The unique characteristics of SPUs make them advantageous for use in biomaterials, structural materials and other applications [1–4]. More than 50 years of research has been dedicated to this field, which has led to a great deal of understanding of the synthesis, structure and properties of these fascinating materials. In general, SPUs possess the structure $-(X—Y)-_n$, composed of a macrodiol "soft" segment (SS) and urethane rich "hard" segment (HS); each segment has a composition incompatible with the other driving phase separation into nanoscale domains, which controls SPUs' properties [5–7]. It is believed that the HSs, either glassy or crystalline with melting temperature (T_m) above ambient temperature, form domains on the order of a few to tens of nanometers. These hard domains separate from the SSs, which are usually formed of either low glass transition temperature (T_g) amorphous or low T_m crystalline segments (T_m less than ambient temperature) [5,7–20].

Extensive research has been performed on the structure–property relationship of SPUs containing aromatic diisocyanates, such as 4,4′-methylenediphenyl diisocyanate (MDI) and 2,6-toluene diisocyanate (TDI), due to their commercial availability and low toxicity [1,5]. It has been shown that mechanical properties can be tailored to range from elastic to plastic by varying the HS content [21,22]. Much of the reported research has focused on SPU compositions containing less than 50 wt.% HS, as many end applications, including sealants, adhesives and elastomers, require materials that are relatively soft. Limited SPU systems containing higher than 50 wt.% aromatic HSs have been reported [14–16]. SPUs that are made of crystallizable HSs and SSs resemble a unique crystalline-crystalline multi-block copolymer where crystallization of each segment provides nanoscale confinement of the other. Confined crystallization has become an interesting research topic in recent years [23–27]. Crystalline polymers and block copolymers have been studied in confined holographically crosslinked polymer matrices [28–30]. Interesting confinement effects have also been observed in polymer nanocomposites [31–34].

The present research investigates the morphology and properties of a crystalline–crystalline SPU, focusing on the confined crystallization behavior of each segment. Poly(ethylene glycol) (PEG) was selected as the polyether macrodiol of our SPUs because it has low transition temperatures and desirable mechanical properties. A variety of molecular weight (MW) PEGs were chosen, because they provide a wide temperature window to conduct confined crystallization studies. An SPU system consisting of 1,6-hexamethlyene

* Corresponding author. Tel.: +1 215 895 2083; fax: +1 215 895 6760.
E-mail address: chrisli@drexel.edu (C.Y. Li).

0032-3861/$ – see front matter © 2010 Elsevier Ltd. All rights reserved.
doi:10.1016/j.polymer.2010.03.027

diisocyanate (HDI) and 1,4-butandiol (BDO) has been synthesized with PEG. Compared with aromatic diisocyanates, the increased chain mobility of the HS, in the present study, will lead to quicker kinetics of phase separation, crystallization, or a combination of both [7,11,12]. Higher HS percent crystallinity has been observed in SPUs with linear, aliphatic HS compared to those made of aromatic diisocyanates [7,11,12]. By using greater than 50 wt.% HS, we were able to study the confining of the SS by a matrix of HS, in opposition to the traditional SPU model in which HSs are dispersed within the SS. It is the focus of this article to report the morphological changes that take place when selectively controlling the crystallization of either the HS or SS, by tailoring the SPU composition.

2. Experimental section

2.1. Materials

PEG, HDI, BDO, *N*,*N*-dimethylacetamide (DMAc) and dibutyltin dilaurate (DBTL) were purchased from Aldrich. PEG of 2000, 4600 and 8000 g/mol MWs were degassed at 80 °C for a minimum of 3 h prior to SPU synthesis. HDI and BDO were vacuum distilled prior to use. DMAc was dried under 0.3 nm molecular sieves for a minimum of three days. DBTL was used as received.

2.2. Polyurethane synthesis

The chemical structure of a typical SPU is shown in Fig. 1. All SPU samples were synthesized using the two step polymerization process using DBTL as a catalyst to facilitate the reaction of the aliphatic diisocyanates [1,35,36].

2.2.1. Synthesis of SPU prepolymer

The SPU prepolymer was synthesized as follows: PEG (15.978 g, 8.0 mmol), DBTL (9.587 mg, 15.1 μmol) and DMAc (85 mL) were added into a 500 mL three- neck flask with a vacuum adapter, condenser, addition funnel and containing a magnetic stir bar. The reaction vessel was kept under a positive pressure of dried nitrogen to prevent water from entering the reactor. A large excess of HDI (10.872 g, 64.7 mmol) in DMAc (~5 mL) was added dropwise into the reaction vessel over ~30 min. The reaction was carried out at 80 °C for 3 h.

2.2.2. Synthesis of high MW SPU

High MW SPU was synthesized as follows: BDO (5.105 g, 56.7 mmol) and DMAc (5 mL) were added concurrently to the prepolymer SPU and HDI mixture at 100 °C dropwise over ~30 min, increased gradually from 80 °C during the prepolymer step. BDO concentrations were based on the balancing of the NCO:OH content to an equal 1:1 molar ratio. The reaction vessel was kept under a positive pressure of dried nitrogen. Polymerization to high MWs was carried out overnight. The polymer solution was collected and precipitated into diethyl ether. The product was filtered and rinsed with a 50:50 (v/v) mixture of ethanol and methanol. The precipitate was dried under vacuum at ~50 °C for one week. ^{1}H NMR(δ, ppm, DMSO-d_6): δ (ppm) = 1.2–1.6 (6H, CH_2), 2.9 (2H, CH_2N), 3.5 (2H, CH_2O), 3.9 (2H, CH_2CO), 7.0 (1H, NH). IR (KBr): 3320 cm^{-1} (NH stretch), 2940 cm^{-1} (asymmetric CH stretch), 2879 cm^{-1} (symmetric CH stretch), 1714 cm^{-1}, 1685 cm^{-1} (amide I), 1541 cm^{-1} (amide II), 1110 cm^{-1} (COC).

2.3. Characterization

Proton nuclear magnetic resonance (^{1}H NMR), Fourier transform infrared spectroscopy (FTIR), differential scanning calorimetry (DSC), wide-angle X-ray diffraction (WAXD), small-angle X-ray scattering (SAXS), dynamic mechanical analysis (DMA) and transmission electron microscopy (TEM) were used to characterize the structure and morphology of the SPUs. The chemical structure of the SPU was analyzed using ^{1}H NMR spectra obtained on a 300 MHz Varian UnityInova with deuterated dimethyl sulfoxide (DMSO-d_6) as the solvent. FTIR spectra were recorded on a Varian Excalibur FTS-3000 using 1wt.% SPU in DMAc cast on potassium bromide (KBr) disks with a 4 cm^{-1} resolution for 128 scans. Intrinsic viscosity was taken using an Ubbelohlde Viscometer with DMAc as the solvent at 70 ± 0.01 °C. Thermal transitions were measured using a PerkinElmer DSC-7 under a constant nitrogen flow. The temperature and heat flow were calibrated using an indium standard at a heating rate of 5 °C/min. Samples with a typical mass of 5 mg were sealed in aluminum pans. An initial

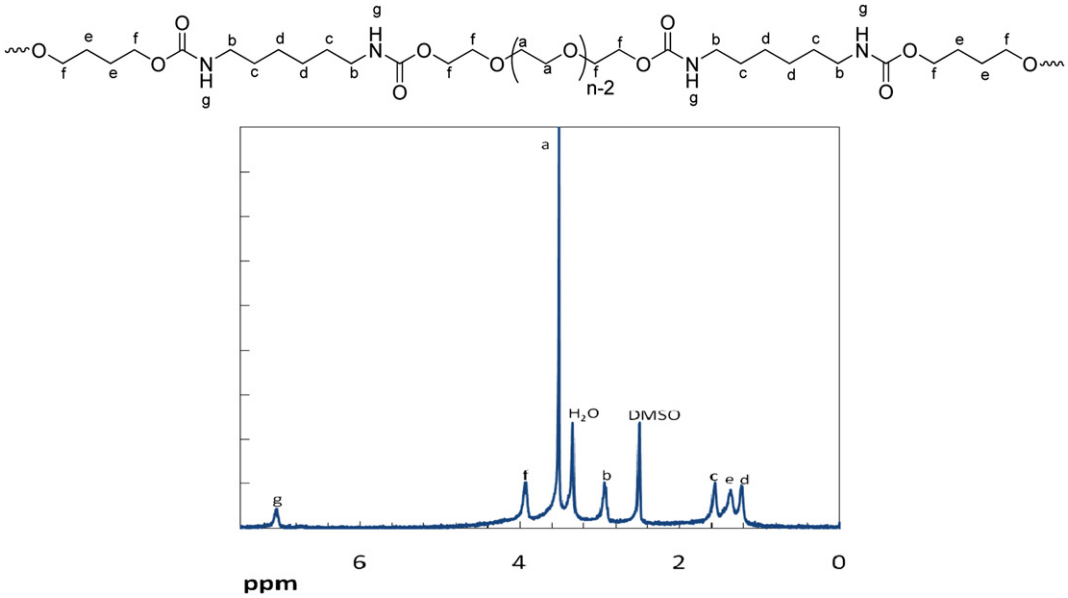

Fig. 1. ^{1}H NMR spectrum of PU47 using DMSO-*d*6 as the solvent.

Table 1
Sample designation, intrinsic viscosity and HS content.

Sample	SS MW (g/mol)	[η] (dl/g)	$\%HS_{feed}$	$\%HS_{calculated}$
PU25	2000	0.266	50	45.08
PU26	2000	0.145	60	65.93
PU45	4600	0.221	50	45.95
PU46	4600	0.118	60	65.23
PU47	4600	0.084	70	75.48
PU85	8000	0.270	50	46.80
PU86	8000	0.192	60	59.45
PU87	8000	0.077	70	76.66

heating to 200 °C was carried out and held isothermally for 1 min to erase all thermal history of the samples. Subsequent cooling and heating were carried out from −20 to 200 °C at 5 °C/min. The first cooling and second heating thermograms are reported. Thermogravimetric analysis (TGA) was performed using a PerkinElmer TGA-7 under nitrogen at a heating rate of 10 °C/min for sample weights between 10 and 15 mg. WAXD was performed using a Siemans D500 diffractometer with a CuKα source and wavelength of 1.54 Å. Scans were taken with a step size of 0.04° and held for 1.0 s. SAXS data was collected with a customized 3 m pinhole collimated SAXS camera. A Rigaku Ultrax18 rotating anode with a copper target was operated at 40 kV/60 mA to generate X-rays with $\lambda = 1.5418$ Å. PU85 and PU86 were melt cast on glass slides at 200 °C and quenched to ambient temperatures. Films had a thickness of ~0.3–0.5 mm. Additional annealing of two PU85 and PU86 films was performed at 60 °C for 3 days. Thermo-mechanical transitions were obtained using a PerkinElmer DMA-7 under nitrogen. Scans were obtained over a temperature range of −150to 200 °C at 3 °C/min with an initial strain of 0.1% and an oscillating frequency of 1 Hz. The morphology of the SPUs were studied using TEM. Images were taken via a CCD camera attached to a JEOL JEM2100 with an accelerating voltage of 200 kV. Samples were prepared via solution casting of 0.1 wt.% SPU in DMAc on carbon coated nickel grids, heated to 200 °C then quenched to 167 °C, near the onset of T_m for the HSs, and allowed to anneal under nitrogen for 48 h to induce HS controlled morphologies. All the samples were shadowed using Pt/Pd before TEM observation, similar to previous reports [37–40].

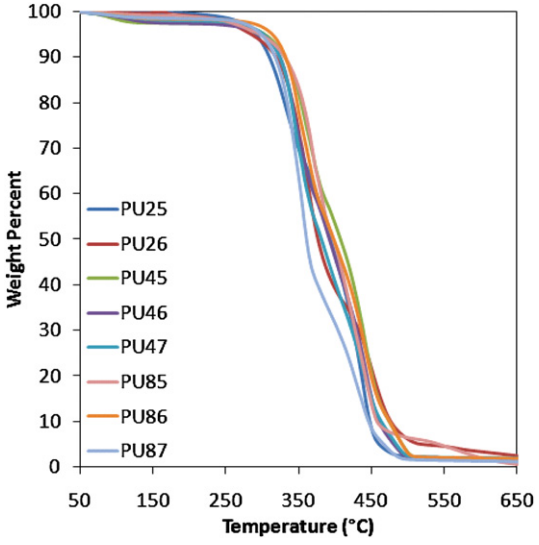

Fig. 2. TGA curves of the PU samples.

3. Results and discussion

3.1. Synthesis and characterization of SPU with high HS contents

Eight polyurethane systems were synthesized using PEG, HDI and BDO of various MWs and concentrations. Samples were designated as PUXY where X indicates the PEG MW and Y the amount of HS, such that PU25 has a PEG MW of 2000 g/mol and 50 wt.% HS. PU2, PU4 and PU8 series will refer to all samples containing 2000, 4600 and 8000 g/mol SSs, respectively. In order to assure significant confinement of the SS crystallization, it was necessary to meet three conditions: a greater volume fraction of HS to SS, a highly crystalline HS or a HS with a high T_g and good separation of the HS and SS. HSs were synthesized at concentrations that were greater than 50 wt.% to ensure that the HS existed in ample amounts to form a dominant crystalline phase, producing confinement of the SS. The chemical structures of the SPU samples were identified using ^{1}H NMR. Fig. 1 shows a ^{1}H NMR spectrum for a typical SPU sample along with the peak relations to hydrogen along the backbone referenced using tetramethylsilane. The labeling of peaks in this way has been used to provide evidence that the samples produced were linear, with no observable crosslinking due to allophanate bond formation or other side reactions that may

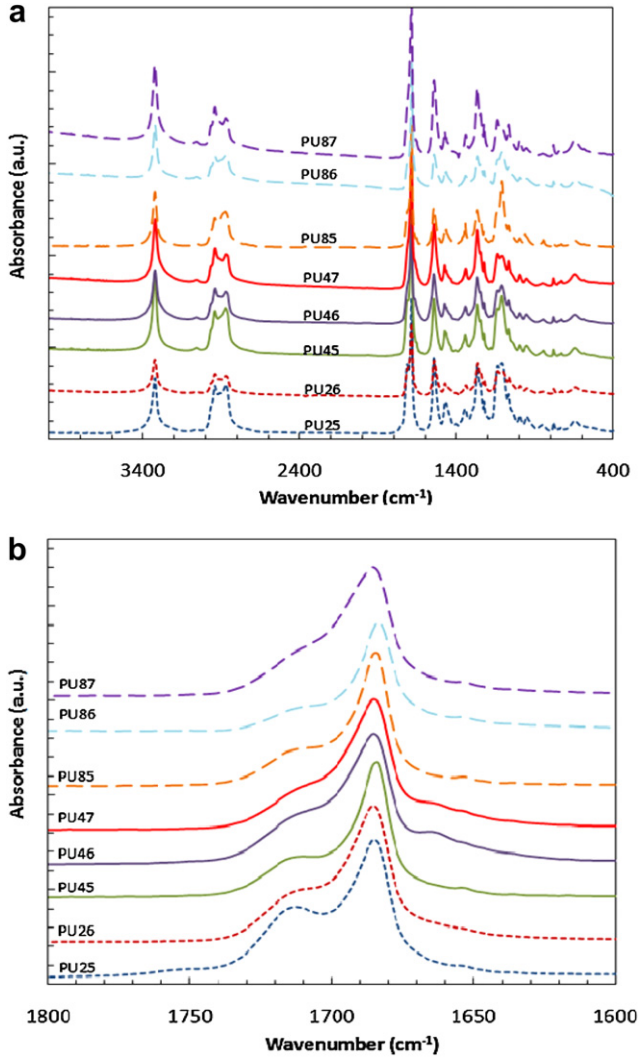

Fig. 3. (a) FTIR spectra of PU samples, (b) expanded FTIR spectra of amide I region.

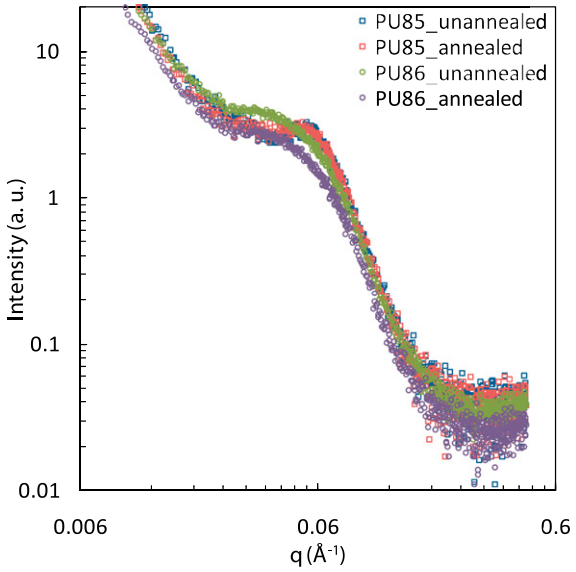

Fig. 4. SAXS of PU85 and PU86 before and after annealing at 60 °C for 3 days.

arise during the synthesis process. Comparing the ratios of the integrated peaks labeled a and b, in Fig. 1, gives an approximate value of the samples' HS content. The values of these ratios were calculated for all samples, listed in Table 1, and are in good agreement with the feed concentration of HS during synthesis [41].

Poor solubility of all synthesized SPU samples required the use of intrinsic viscosity to get a relative relationship to sample MW. Measurements were taken using DMAc as the solvent at 70 °C. The intrinsic viscosity is related to MW by the Mark–Houwink–Sakurada equation.

$$[\eta] = KM^a$$

Parameters K and a are dependent on factors including polymer composition, polymer–solvent interactions and temperature. Table 1 shows the intrinsic viscosities calculated for the SPU series. As HS content increases there is a general decrease in the intrinsic viscosity due to reduced flexibility of the chains and lower solubility of the SPU in the DMAc as a result of a greater degree of hydrogen bonding within the HS. MWs of the SS did not apparently affect the intrinsic viscosity. There have been no data reported on the parameters K and a for SPUs with the aforementioned compositions and experimental conditions; therefore, a direct comparison of intrinsic viscosity to MW is difficult. Nevertheless, the listed intrinsic viscosities from Table 1 are similar to those observed for a number of SPU systems in the literature, corresponding to a relatively high MW [42].

TGA scans of the SPU series were collected under nitrogen at 10 °C/min to detail the thermal degradation (Fig. 2). All samples showed a 5 wt.% loss at ~285–314 °C. Differential weight loss curves showed two main peaks with T_{1max} at ~340–370 °C and T_{2max} of ~423–351 °C. The former is attributed to the greatest rate of mass loss of the HS while the later accounts for the greatest rate loss of SS mass [43].

FTIR was used to probe the composition of the SPU and determine the relative degree of phase separation due to thermodynamics, mobility and crystallization [5,44]. The FTIR spectra in Fig. 3a suggest a composition that is in agreement with the ^{1}H NMR data. Distinct bands related to amine, asymmetric and symmetric methylene, carbonyl, and PEG ether were observed at 3320, 2940 and 2879, 1714 and 1685, and 1110 cm^{-1}, respectively. The lack of an isocyanate peak at 2250 cm^{-1} and the presence of the amine and carbonyl peaks indicate a complete conversion of monomers to urethane. The two peaks attributed to methylene at 2940, 2879 cm^{-1} can be attributed to asymmetric CH stretching and symmetric CH stretching respectively. For all samples with 50 wt.%

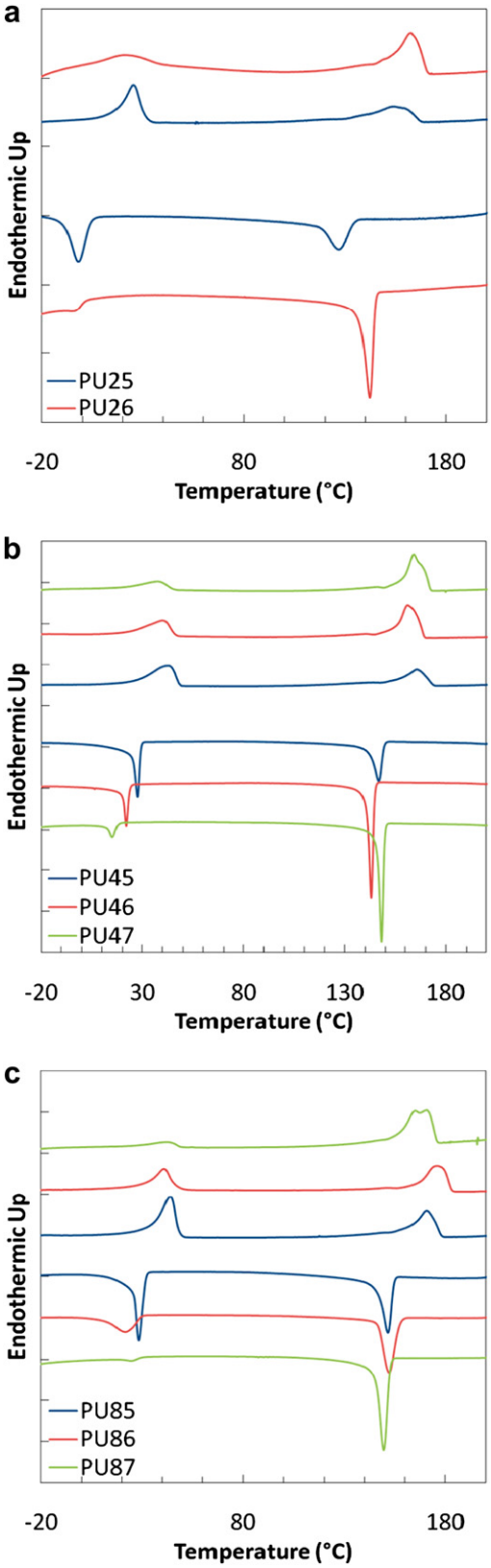

Fig. 5. DSC endotherms of (a) PU2 series, (b) PU4 series, and (c) PU8 series.

HS content, the peak at 2940 cm^{-1} possessed a lower intensity than the peak at 2879 cm^{-1}. It was observed that as the HS content was increased beyond 50%, a shift in relative peak intensity followed such that the peak at 2940 cm^{-1} becomes stronger than the 2879 cm^{-1} peak.

The present system is a crystalline–crystalline block copolymer, and so, it must be noted that the strong drive towards crystallization within the HDI–BDO HS further adds to the degree of phase separation by excluding the SS from the crystalline HS domain, complicating the physical chemistry model for phase separation. The extent of hydrogen bonding of the urethane carbonyl can approximate the degree of phase separation. The extent and type of hydrogen bonding can be inferred by observing the intensities of the carbonyl "shoulder" at 1714 cm^{-1} and of the PEG peak and its breadth at 1110 cm^{-1}. The peak at 1685 cm^{-1}, due to carbonyls that are organized and strongly hydrogen bonded to amines, possess restricted vibrational motions registered by a lower absorbed frequency. It has been reported that the carbonyl peak can be separated into three regions, related to different types of hydrogen bonding in SPU. Carbonyl not involved in hydrogen bonding have peaks that were observed near 1732 cm^{-1}, carbonyl associated with poorly ordered hydrogen bonding were observed at 1708 cm^{-1} and strongly hydrogen bonded carbonyl were observed around 1685 cm^{-1} [5,44,45]. Accordingly, we attribute the 1685 and 1714 cm^{-1} bands for 50 wt.% HS SPUs to strong and poorly hydrogen bonded carbonyl, respectively (Fig. 3b). The slight deviations from the aforementioned peak positions reported in the literature are due to differences in the HS components. As HS content increases, the carbonyl peak at 1685 cm^{-1} broadened due to the formation of larger HS domains. In addition, with increasing HS content the peak around 1714 cm^{-1} not only shows some suppression but also downshifts, overlapping with the stronger hydrogen bonded peak, as shown in Fig. 3b. This can be attributed to an increased degree of phase separation with increasing HS content.

The amine peak at 3320 cm^{-1} appears to be narrow and relatively symmetric. If phase mixing were prevalent, a shoulder on the high-frequency side of the 3320 cm^{-1} band would appear, related to free amine and the full-width at half-maximum would be broad, which was not observed [5,44,45]. This suggests that there was no significant number of free amines to be detected by FTIR.

Formation of the HS and SS domains, as was discussed previously, is a result of thermodynamic and kinetic properties of the segmented chains, resulting in phase separation. Fig. 4 shows the SAXS of PU85 and PU86 for samples quenched from the melt and those that were annealed at 60 °C, above T_m of the SS, for 3 days. Subtraction of the baseline produces peaks that were fitted to a Lorentzian distribution. The *d*-spacing of the HS/SS separation was found to be 11.1 and 14.3 nm for PU85 and PU86, respectively. The annealing process did not change the spacing. PU86 samples have a larger domain size than their corresponding PU85 which is consistent with that PU86 possesses ~10 wt.% more HS than PU85.

3.2. Structure and morphology of SPU with high HS contents

Fig. 5 shows the DSC thermograms of SPU samples based on 2000, 4600 and 8000 g/mol PEG. The second heating shows two clear endotherms, attributed to the T_m of the SS and HS. For all samples containing 50 wt.% HS, a broad peak of the HS endotherm is observed. As the HS content is increased, the HS endotherm peak shifts and appears to have multiple endotherms. It has been shown that the semi-crystalline HS can possess multiple endotherm transitions depending on the degree of phase mixing and the HS length uniformity created during synthesis [8,14–16,46]. It is possible for the HS to possess a T_g, which is often reported within the range of 90–120 °C for many aromatic diisocyanates. However, no T_g was seen for our samples at a heating rate of 5 and 40 °C/min, not shown, due to their relatively high degree of crystallization and small change in heat capacity [47]. Table 2 shows a summary of the results of the DSC thermograms for all the samples. Pure PEG was evaluated by Wunderlich et al. and was shown to possess a heat of fusion (ΔH_f) of 8.66 kJ/mol while the work of Kajiyama and MacKnight found that the HDI–BDO HSs' possess a ΔH_f of 48.53 kJ/mol [48,49]. The crystallinity of the samples was determined by comparing the area under the samples soft and hard segment endotherms as a fraction of the values determined for 100% crystallinity [50].

A 5–14 °C decrease in the SS $T_{onset,c}$ with increasing HS content was observed. The area of the $T_{onset,c}$ peak is observably decreased with increasing HS content, to the extent of almost being suppressed for 70 wt.% HS content samples. A good portion of the sample's SS is therefore amorphous. On the other hand, the crystallinity of the HSs was also drastically reduced compared with the pure HS PU. This is attributed to the "soft confinement effect" in which a certain degree of phase mixing between the HS and SS occurs, which in turn, decreases the HS crystallinity.

The crystal structures of the SPU samples were analyzed using WAXD using both quenched and annealed samples. Fig. 6 shows the crystal reflection peaks for samples quenched to room temperature after being heated for 5 min at 200 °C. Diffraction peaks belonging to monoclinic PEG crystals and triclinic HDI-BDO crystals can be identified [23,51–54]. We observed a PEG peak with a *d*-spacing of 0.463 nm attributed to the (1 2 0) plane reflection and another at a *d*-spacing of 0.380 nm. 7 planes for PEG can be associated with a *d*-spacing near 0.380 nm; ($\bar{1}$32), (032), (112), ($\bar{2}$12), (124), ($\bar{2}$04), (004) [23]. HDI–BDO was observed to have

Table 2
Thermal transitions and degree of crystallinity of SPUs measured by DSC.

Sample	Soft segment				Hard segment			
	$T_{onset,m}$ (°C)	$T_{onset,c}$ (°C)	ΔH_m (J/g)	%Cryst.	$T_{onset,m}$ (°C)	$T_{onset,c}$ (°C)	ΔH_m (J/g)	%Cryst.
PEG-2000	49.44	38.75	166.53	84.61	–	–	–	–
PEG-4600	57.47	34.34	150.80	76.62	–	–	–	–
PEG-8000	61.24	38.86	156.94	79.74	–	–	–	–
HDI-BDO	–	–	–	–	167.98	152.68	119.50	63.57
PU25	16.56	4.35	59.04	30.00	131.95	133.68	54.44	28.96
PU26	10.18	0.86	22.72	11.54	151.72	145.03	57.90	30.80
PU45	26.97	29.26	75.82	38.52	155.35	149.52	68.77	36.58
PU46	22.64	23.60	66.58	33.83	154.62	144.77	79.18	42.12
PU47	24.90	17.77	55.74	28.32	158.05	149.83	76.37	40.62
PU85	34.85	31.85	82.08	41.70	160.82	154.54	71.68	38.13
PU86	31.85	29.75	78.36	39.81	165.25	157.20	78.28	41.64
PU87	33.76	29.66	15.37	7.81	157.37	152.75	77.16	41.04

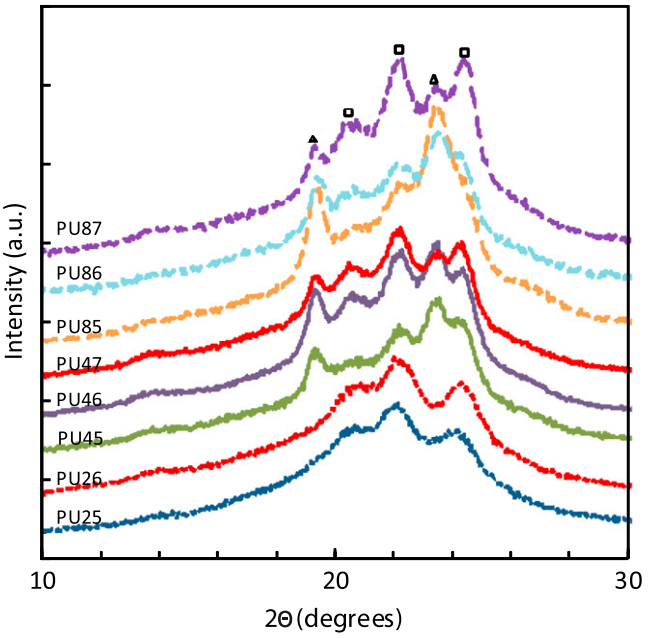

Fig. 6. WAXD for samples quenched to room temperature after 5 min at 200 °C. Squares – HDI–BDO peaks; triangles – PEG peaks.

three peaks with *d*-spacings of 0.431 nm associated with the (100) plane, 0.400 nm with the $(\bar{1}10)$ plane, and 0.364 nm with the $(\bar{1}11)$ plane [52]. The peak intensities differ significantly in these eight samples. The well-defined peaks that arose in samples quenched from the melt to room temperature are indicative of the fast crystallization/phase separation kinetics of the samples compared to aromatic diisocyanate systems, which show only a broad peak associated with crystallinity for most samples quenched to room temperature. HDI and BDO are both linear and aliphatic, and have greater mobility compared to the more commonly used HSs MDI and TDI. This increased mobility therefore instills a quicker and more complete phase separation.

For both PU25 and PU26, PEG diffractions are negligible while the three peaks of the HS diffraction can be identified, indicating that HSs crystallized during the quenching process. The absence of the PEG peak is consistent with the DSC observation that the T_m of the SSs in PU25 and PU26 are below ambient temperature. For the PU4 series, we observe both SS and HS reflections, indicating both segments crystallized upon quenching. Furthermore, the relative intensity of the HS and the SS diffractions changed dramatically as the HS content was increased from 50 to 70 wt.%. In PU45, the SS diffraction clearly dominates while in PU47, the intensity of HS diffraction is stronger. More evident observation can also be seen in the PU8 series. In PU85, negligible HS diffraction can be observed while in PU87 the diffraction peaks of HS are much stronger than that of the SS diffraction; this observation clearly demonstrates the interplay of HS and SS crystallization during the fast quenching process. In the PU2 series, since the SS is liquid at ambient temperature, the phase morphology is controlled by the HS crystallization during quenching. Because the quenching process is fast, relatively poor HS crystals were formed evidenced by the broad diffraction peaks in Fig. 6. For both the PU4 and PU8 series, the SS crystal peaks intensity significantly decreased while HS crystal peaks intensity increased upon increase of the HS concentration, indicating that higher HS contents led to a more crystalline HS domain. These crystalline HS domains apparently imposed stronger confinement upon SSs crystallization.

In order to further study the kinetics of the confinement effect on the SS, each sample was heated at 200 °C for 5 min and then cooled to room temperature at 1 °C/min. The effect of this change in thermal history on the crystal structure of the SPU samples is drastic. The slow cooling rate allows the HS to crystallize more fully before the SS. The WAXD patterns of the slow-cooled samples are shown in Fig. 7. The peaks related to the HS show marked intensity gains. For the PU2 series, the HS diffraction peaks' intensities dramatically increased while no SS diffractions can be observed, due to the low T_m of the SS crystals. For PU45 and PU85, we can see clear differences of the relative intensity of the HS and SS diffractions compared with the quenched samples. In the quenched sample, as previously shown, SS crystallization dominated and the degree of crystallinity of the HS was small. However, as shown in Fig. 7, the relative peak intensities of the HS and SS diffractions are comparable, indicating that slow cooling allowed the HS enough time to crystallize. The confinement effect of the slowly formed HS crystals on the SS crystallization is more evident in SPUs with higher HS contents. While we observed appreciable SS crystallization in the quenched PU87 and PU47, the degree of the SS crystallinity was dramatically reduced in the slow-cooled PU46 and PU86 and is completely suppressed in PU47 and PU87, indicating that better packed HS crystals impose stronger confinement effect on SS crystallization.

TEM experiments were conducted on PU85. Thin film samples were solution cast on carbon coated TEM grids and annealed at 167 °C for approximately 48 h. PU85 was chosen for its relatively high SS MW and lower HS content, compared to other samples in the series. The primary structure observed under the TEM was spherulites composed of fibrillar/needle-like crystals and is shown in Fig. 8. Recently, Wilkes et al. reported the observation of fibrillar structures in a series of poly(tetramethylene oxide)-based SPUs,

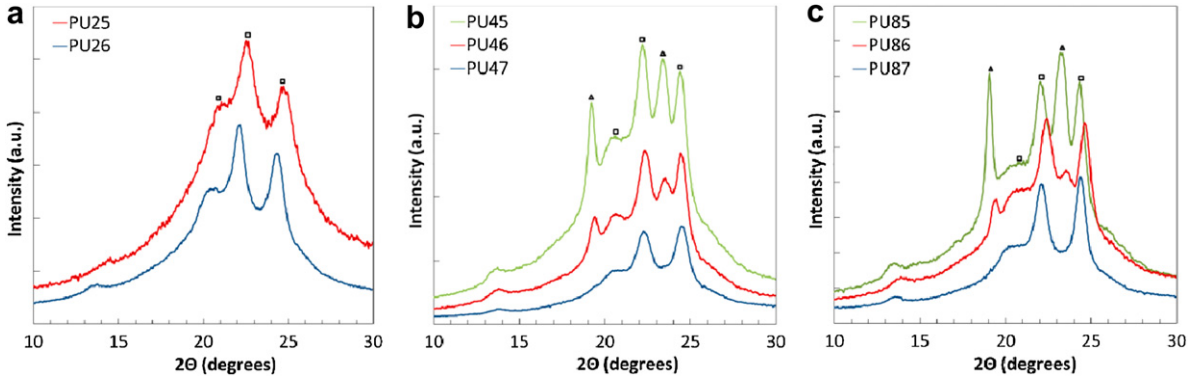

Fig. 7. WAXD for samples cooled to room temperature at 1 °C/min from 200 °C. Squares – HDI–BDO peaks; triangles – PEG peaks.

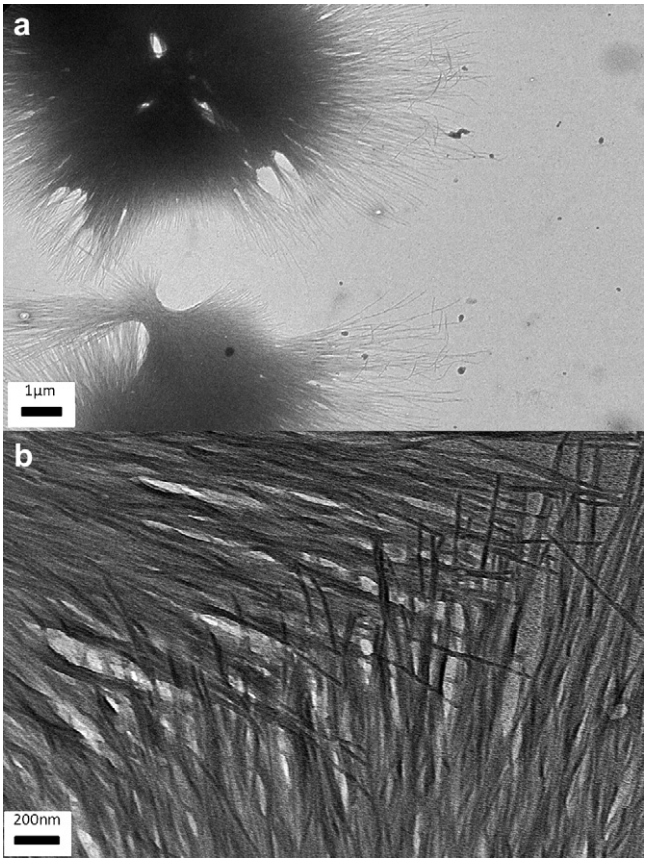

Fig. 8. TEM images of PU85 spherulites with needle-like single crystals. (a) low and (b) high magnification.

where the HS lengths were well controlled [55,56]. Similar morphologies were later observed using AFM in a few groups [17,18]. Most of these works were conducted on solution cast, relatively thick films and the fibrillar morphology was in general attributed to the phase separation of HSs and SSs, while Wilkes et al. did report the relationship between the orientation between the fibrillar structure and the spherulites. Our TEM images clearly show the development of spherulites: the needles are parallel to the radial direction of the spherulites. More interestingly, Popoff eyes were observed, as shown in Fig. 8a, indicating that the branching of the needle crystals is the formation mechanism of the PU spherulites. The needle crystals are apparently a few tens of micrometers long and their width is well defined – approximately 5–7 nm. Fig. 8b is of particular interest: this is an enlarged area where two spherulites impinge. The needle crystals belonging to different spherulites penetrated through the boundary and continuously grew into the adjacent spherulites. The overlap region is on the order of a few hundreds of nanometers to micrometers. This interpenetrating morphology could be of particular interest for mechanical properties as the boundary regions should be dramatically strengthened.

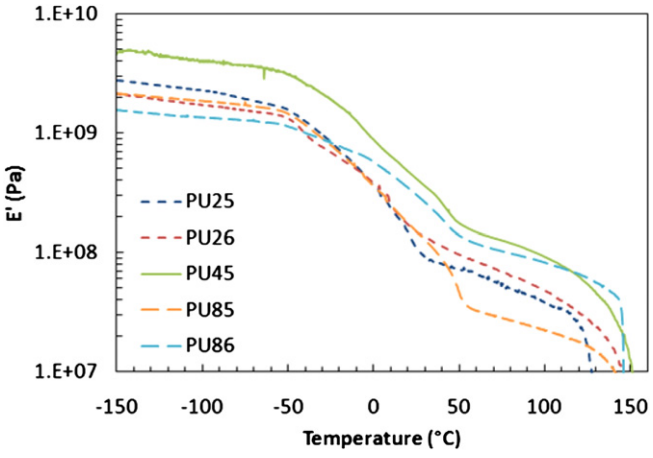

Fig. 9. Storage modulus of SPUs at different temperatures measured by DMA.

Table 3
Storage moduli of SPU samples, at various temperatures.

Sample	Storage modulus (MPa)			
	−100 (°C)	0 (°C)	25 (°C)	100 (°C)
PU25	2300	358	108	37.9
PU26	1720	380	147	47.8
PU45	4070	887	417	92.3
PU85	1860	358	149	22.0
PU86	1360	582	306	82.5

3.3. Dynamic mechanical analysis of SPU with high HS contents

The dynamic mechanical behaviors of the SPU samples were used to investigate thermal transitions and material stiffness. Five of the samples, PU25, PU26, PU45, PU85 and PU86 were tested. Fig. 9 shows the storage modulus *E'* versus temperature. Average *E'* of the samples ranged from ~1.3 to 4.1 GPa for −100 °C and from 108 to 417 MPa for room temperature (Table 3), consistent with the literature data [18].

The first decrease in modulus is broad, spanning from −50 to ~50 °C. This decrease is due to two transitions, the glassy to rubbery transition above the SS T_g and melting of the SSs above the SS T_m. The decrease in storage moduli is approximately one order of magnitude, which is significantly less than most SPUs reported. This can be ascribed to the high HS contents in our samples which are still robust over the range of temperatures in the first transition. After melting of the SS, the samples exhibited elastomeric properties. A slight decrease in moduli, with increasing temperature, is attributed to PEG chain deformation with the higher MW PEG showing the smallest decrease in slope in the elastomeric range. Final failure of the polymer occurred around the T_m of the HS which differed from the DSC data mostly due to processing conditions.

4. Conclusions

A series of HDI–BDO–PEG based SPU samples, with high HS content, was synthesized. The SPU series rapidly phase separated into PEG and HDI–BDO domains and represents a class of crystalline-crystalline block copolymers. Confined crystallization of both HS and SS was studied. As HS content increased, there was a marked decrease in SS crystallinity suppressed by the crystalline HS domain that near to the SS domains. SPU spherulites with unique needle-like crystals parallel to the radial direction of the spherulites were observed using TEM. This study demonstrates that control of HS and SS content in SPUs has the potential for tailoring mechanical properties for structural and impact absorbing materials.

Acknowledgment

We thank the US Army Research Laboratory for financial support under the Army Materials Center of Excellence Program (Contract W911NF-06-2-0013) and the Department of Education's GAANN DREAM Fellowship. WAXD, FTIR and TEM experiments were carried out at Drexel's Centralized Research Facility.

References

[1] Szycher M. Szycher's handbook of polyurethanes. Boca Raton: CRC Press LLC; 1999.
[2] Hepburn C. Polyurethane elastomers. 2nd ed. London and New York: Elsevier Applied Science; 1992.
[3] Oertel G. Polyurethane handbook. Ohio: Hanswer/Garnder Publications, Inc.; 1993.
[4] Chattaopadhyay DKN, Raju KVSN. Prog Polym Sci 2007;32:352–418.
[5] Petrovic ZS, Ferguson J. Prog Polym Sci 1991;16:695–836.
[6] Koberstein JT, Stein RS. J Polym Sci Part B Polym Phys 1983;21:1439–72.
[7] Li YJ, Gao T, Chu B. Macromolecules 1992;25:1737–42.
[8] Koberstein JT, Galambos AF. Macromolecules 1992;25:5618–24.
[9] Koberstein JT, Galambos AF, Leung LM. Macromolecules 1992;25:6195–204.
[10] Koberstein JT, Leung LM. Macromolecules 1992;25:6205–13.
[11] Li YJ, Gao T, Liu J, Linliu K, Desper CR, Chu B. Macromolecules 1992;25:7365–72.
[12] Chu B, Gao T, Li YJ, Wang J, Desper CR, Byrne CA. Macromolecules 1992;25:5724–9.
[13] Desper CR, Byrne CA, Li YJ, Chu B. Macromolecules 1995;28:4213–26.
[14] Saiani A, Daunch WA, Verbeke H, Leenslag JW, Higgins JS. Macromolecules 2001;34:9059–68.
[15] Saiani A, Novak A, Rodier L, Eeckhaut G, Leenslag JW, Higgins JS. Macromolecules 2007;40:7252–62.
[16] Saiani A, Rochas C, Eeckhaut G, Daunch WA, Leenslag JW, Higgins JS. Macromolecules 2004;37:1411–21.
[17] Korley LTJ, Liff SM, Kumar N, McKinley GH, Hammond PT. Macromolecules 2006;39:7030–6.
[18] Korley LTJ, Pate BD, Thomas EL, Hammond PT. Polymer 2006;47:3073–82.
[19] Waletzko RS, Korley LTJ, Pate BD, Thomas EL, Hammond PT. Macromolecules 2009;42:2041–53.
[20] Chau KW, Geil PH. Polymer 1985;26:490–500.
[21] Sarva SS, Deschanel S, Boyce MC, Chen WN. Polymer 2007;48:2208–13.
[22] Sarva SS, Hsieh AJ. Polymer 2009;50:3007–15.
[23] Loo YL, Register RA, Ryan AJ. Macromolecules 2002;35:2365–74.
[24] Zhu L, Cheng SZD, Calhoun BH, Ge Q, Quirk RP, Thomas EL, et al. J Am Chem Soc 2000;122:5957–67.
[25] Hu WB, Cai T, Ma Y, Hobbs JK, Farrance O, Reiter G. Faraday Discus 2009;143:129–41.
[26] Li CY, Ge JJ, Bai F, Calhoun BH, Harris FW, Cheng SZD, et al. Macromolecules 2001;34:3634–41.
[27] Woo E, Huh J, Jeong YG, Shin K. Phys Rev Lett 2007;98:4.
[28] Li CY, Birnkrant MJ, Natarajan LV, Tondiglia VP, Lloyd PF, Sutherland RL, et al. Soft Matter 2005;1:238–42.
[29] Birnkrant MJ, McWilliams HK, Li CY, Natarajan LV, Tondiglia VP, Sutherland RL, et al. Polymer 2006;47:8147–54.
[30] Birnkrant MJ, Li CY, Natarajan LV, Tondiglia VP, Sutherland RL, Lloyd PF, et al. Nano Lett 2007;7:3128–33.
[31] Li CY, Li L, Cai W, Kodjie SL, Tenneti KK. Adv Mater 2005;17:1198–202.
[32] Li L, Li B, Hood MA, Li CY. Polymer 2009;50:953–65.
[33] Li L, Yang Y, Yang G, Chen X, Hsiao BS, Chu B, et al. Nano Lett 2006;6:1007–12.
[34] Dillon DR, Tenneti KK, Li CY, Ko FK, Sics I, Hsiao BS. Polymer 2006;47:1678–88.
[35] Luo S, Tan H, Zhang J, Wu Y, Pei F, Meng X. J Appl Polym Sci 1997;65:1217–25.
[36] Ni H, Nash HA, Worden JG, Soucek MD. J Polym Sci A Polym Chem 2002;40:1677–88.
[37] Li CY, Yan DH, Cheng SZD, Bai F, He TB, Chien LC, et al. Macromolecules 1999;32:524–7.
[38] Li CY, Cheng SZD, Ge JJ, Bai F, Zhang JZ, Mann IK, et al. J Am Chem Soc 2000;122:72–9.
[39] Li CY, Yan DH, Cheng SZD, Bai F, Ge JJ, Calhoun BH, et al. Phys Rev B 1999;60:12675–80.
[40] Li CY, Cheng SZD, Ge JJ, Bai F, Zhang JZ, Mann IK, et al. Phys Rev Lett 1999;83:4558–61.
[41] Asplund JOB, Bowden T, Mathisen T, Hilborn J. Macromolecules 2006;39:4380–5.
[42] Chen CT, Eaton RF, Chang YJ, Tobolsky AV. J Appl Polym Sci 1972;16:2105–14.
[43] Petrovic ZS, Zavargo Z, Flynn JH, MacKnight WJ. J Appl Polym Sci 1994;51:1087–95.
[44] Yilgor I, Yilgor E, Guler IG, Ward TC, Wilkes GL. Polymer 2006;47:4105–14.
[45] Sonnenschein MF, Lysenko Z, Brune DA, Wendt BL, Schrock AK. Polymer 2005;46:10158–66.
[46] Koberstein JT, Russell TP. Macromolecules 1986;19:714–20.
[47] Camberlin Y, Petrovic JP. J Polym Sci Polym Phys Ed 1984;22:1835–44.
[48] Kajiyama T, MacKnight WJ. Polym J 1970;1:548–54.
[49] Suzuki H, Grebowicz J, Wunderlich B. Makromol Chem 1985;186:1109.
[50] Seymour RW, Cooper SL. Polym Lett 1971;9:689–94.
[51] Chen-Tsai CHY, Thomas EL, MacKnight WJ, Schneider NS. Polymer 1986;27:659–66.
[52] Saito Y, Nansai S, Kinoshita S. Polym J 1972;3:113–21.
[53] Blackwell J, Gardner KH. Polymer 1979;20:13–7.
[54] Briber RM, Thomas EL. J Polym Sci Polym Phys Ed 1985;23:1915–32.
[55] Aneja A, Wilkes GL. Polymer 2003;44:7221–8.
[56] Sheth JP, Wilkes GL, Fornof AR, Long TE, Yilgor I. Macromolecules 2005;38:5681–5.